A&A 490, 393–402 (2008)
DOI: 10.1051/0004-6361:200810495

Astronomy & Astrophysics

Non-gravitational motion of the Jupiter-family comet 81P/Wild 2

II. The active regions on the surface

S. Szutowicz[1], M. Królikowska[1], and H. Rickman[1,2]

[1] Space Research Centre of the Polish Academy of Sciences, Bartycka 18A, 00-716 Warsaw, Poland
e-mail: slawka@cbk.waw.pl
[2] Astronomical Observatory, Box 515, 75120 Uppsala, Sweden

Received 1 July 2008 / Accepted 30 July 2008

ABSTRACT

Aims. The non-gravitational perturbations in the orbital motion of comet 81P/Wild 2 are investigated using a two-source model of outgassing.
Methods. In the process of orbit improvement the nucleus orientation and the location of two active regions are found from numerical fitting of the non-gravitational acceleration model to positional observations of the comet. Two different approaches to the lag angle of the outgassing behind the subsolar meridian are considered, assuming this angle to be either constant or varying with heliocentric distance.
Results. The derived spin axis orientation ($I \sim 60°$, $\phi \sim 155°$) as well as the location of two active regions, the northern ($\beta = 84°$) and the southern one ($\beta = -42°$), agree with determinations based on different observations by other authors. Orbital linkages of two and three successive apparitions of 81P/Wild 2 indicate an evolution of the change in the orbital period, possible time variations of the spin axis of the comet and an increase of the source areas during the last five revolutions. The non-gravitational perturbations were also used to constrain the sizes of the two active areas as well as the mass and bulk density (~400 kg m^{-3}) of the comet nucleus. The modeled two-source water production curve is compared with the activity data represented by the observed water production curve and the brightness curve.

Key words. comets: individual: 81P/Wild 2

1. Introduction

Direct indications of anisotropic emission and possible active regions on the surface of a cometary nucleus come from jets, fans and other distinctive structures observed in the comae. The non-uniform activity of a cometary nucleus, where the surface is characterized by active and inactive areas, may result in a perihelion asymmetry of the gas production curve as well as in an asymmetric variation of the non-gravitational force perturbing the cometary orbit. Comet 81P/Wild 2 exhibits both these features.

The comet was discovered in 1978 in a short-period orbit typical for the Jupiter-family comets, and to date it has been observed at all five returns to perihelion. However, shortly before its first apparition the comet moved much further from the Sun in an orbit with perihelion at ~5.0 AU and aphelion at ~19 AU. The comet was injected into the inner part of the Solar System during an extremely close approach to within 0.0061 AU of Jupiter in September 1974. Thus the orbit changed dramatically. The perihelion distance decreased to 1.49 AU, and the orbital period decreased from more than 40 years to 6.2 years (currently 6.4 yrs).

Before the encounter with Jupiter the orbit of the comet was stable for at least 300 years (Królikowska & Szutowicz 2006, hereafter Paper I). Our long-term orbital calculations showed that the orbital history of the comet is well defined only within about 300 years in the past and 250 years in the future, while outside this interval the dynamical evolution starts to become unpredictable. In Paper I we investigated the past and future dynamical evolution of 81P/Wild 2 – within a time frame of ±8000 years – in a statistical sense on the basis of positional observations from all five apparitions, taking into account the non-gravitational perturbations. We considered both symmetric and asymmetric non-gravitational models. In a set of one hundred randomly selected orbits fitted with the same accuracy to the positional observations of the comet, 74% of the orbits evolve backwards into perihelion distances larger than 4 AU, and only 9% of the orbits acquire perihelion distances less than 2 AU. Thus, although somewhat unlikely, the possibility that in the past the comet has been residing in the inner Solar System and experiencing insolation that modified the near surface layers cannot be excluded.

The primary landmark in the history of investigation of comet 81P/Wild 2 was the *Stardust* mission with its close flyby in January 2004. Images of the nucleus taken during this flyby revealed a very complex surface morphology with several sharp features (Brownlee et al. 2004). Many detailed inferences can be made, and for instance, the chaotic topography of the surface may indicate internal inhomogeneities of the nucleus structure, while some landforms may bear witness of surface erosion due to sublimation.

A detailed modeling of the sublimation-induced non-gravitational force for 81P/Wild 2 based on thermophysical models was performed by Davidsson & Gutiérrez (2006). The authors established upper limits for the mass and bulk density of the nucleus as $M \lesssim 2.3 \times 10^{13}$ kg and $\rho_{\rm bulk} \lesssim 600$–$800$ kg m^{-3}, respectively. Gutiérrez & Davidsson (2007) studied the possible variations of the spin axis orientation. In both papers the nucleus was modeled as a triaxial ellipsoid or irregularly shaped body

Table 1. Characteristics of positional observations of comet 81P/Wild 2.

Perihelion time	Observation interval	Number of obs.	Number of res.	Mean res.	q [AU]	e
1978 June 15	1978 Jan. 6–1979 June 27	177	352	1.″13	1.491	0.5567
1984 Aug. 20	1983 Sep. 18–1986 Sep. 26	94	179	1.″43	1.494	0.5561
1990 Dec. 17	1988 Sep. 9–1992 Aug. 2	97	159	0.″60	1.572	0.5420
1997 May 6	1995 Jan. 2–1998 Sep. 16	234[a]	458[a]	0.″60	1.583	0.5402
2003 Sep. 26	2002 Sep. 5–2004 Aug 7	228[a]	439[a]	0.″60	1.590	0.5387

[a] The numbers of residuals for the two most recent apparitions have been reduced by using normal places for some observations.

covered by various surface activity maps, which reproduce the observed water production rate and non-gravitational changes of the orbit.

Prior to Stardust, Sekanina (2003) determined the spatial orientation of the spin axis and the latitudes of two active discrete emission sources based on the dust coma features and their temporal evolution as observed during the comet's apparition in 1997. Two-jets activity was confirmed by Farnham & Schleicher (2005) based on both narrowband photometry and CCD imaging of the comet.

In the present paper we concentrate on the non-uniform activity of the comet. We consider two discrete sources of outgassing attributed to the local sublimation of exposed water ice. To derive the spin axis orientation, the locations and the relative sizes of the active regions, we find a fit to the astrometric observations of the comet by integrating its equations of motion, including a non-gravitational acceleration modeled as a function of the mentioned physical parameters. The model used for this purpose is that described by Szutowicz (2000). We also make use of the light curves and water production rate measurements for 81P/Wild 2 to constrain the mass of the nucleus and the areas of the active regions.

2. Method of calculations and observational material

The equations of motion of the comet and the planets are integrated numerically using the recurrent power series method (Sitarski 1989, 2002), including directly the non-gravitational terms. The orbital elements and the non-gravitational parameters specific for a given model (see Sects. 3 and 4) are determined from the observational equations by the least squares method in an iterative process of orbit improvements (Sitarski 1984).

2.1. Positional observations

The orbital calculations are based on the positional observations of comet 81P/Wild 2. The total material contains 2262 observations made between 1978 January 6 and 2004 August 7. The number of observations from the last two apparitions is much larger than from the others. To give each apparition roughly equal weight in the solutions we introduced normal places for these apparitions. Thus the collected observations were reduced into 830 sets and selected according to mathematical criteria (for details see Paper I).

The global characteristics of the positional observations are listed in Table 1. The last two columns of the table indicate the perihelion distance, q, and eccentricity, e, at each apparition. The quality of the observations at each apparition is represented by the mean residual resulting from a purely gravitational model of the orbital motion. A similar measure of the quality of the observational material over several apparitions – an "a priori" mean residual – can be constructed from the whole set of observations, combining the residuals of the single apparitions in a way described e.g. by Szutowicz & Rickman (2006). This represents a limiting error which the linkages aim to reproduce as well as possible. "A priori" residuals for a few sets of comet returns are presented in Table 2. The present orbital calculations are mostly based on observations from 1983 Sep. 18 to 2004 Aug. 7 covering the last four apparitions of the comet.

Table 2. The limiting errors calculated for several periods of time spanning a few apparitions.

Interval	Number of obs.	Number of res.	Mean res.
1978–1984–1990–1997–2003	830	1587	0.″87
1978–1984–1990	368	690	1.″13
1984–1990–1997	425	796	0.″86
1984–1990–1997–2003	653	1235	0.″78
1990–1997	331	617	0.″60
1990–1997–2003	559	1056	0.″60
1997–2003	462	897	0.″60

2.2. Photometric data

Magnitude estimates of comet 81P/Wild 2 have been taken from the International Comet Quarterly archive of photometric data (Smithsonian Astrophysical Observatory, Cambridge, MA), in electronic form (Green 1991, 1997). In this study we only consider brightness profiles for the 1990 and 1997 apparitions. The apparitions in 2003 and 1984 were too unfavorable to use the corresponding data. For the 1978 apparition the observations cover only 122 days before perihelion.

To derive a light curve $m_H(t)$, describing the heliocentric magnitude as a function of the time from perihelion, we corrected the apparent magnitudes for the geocentric distance. In the next step we selected brightness estimates applying corrections for personal and instrumental effects according to the procedure described in Szutowicz & Rickman (2006). In general we derived the observer specific corrections comparing observations made within two days by different observers and telescope types.

The brightness curve for 1990 is based on 80 selected magnitude estimates made by nine observers from 63 days before to 230 days after perihelion. For the 1997 apparition a total number of 219 measurements made by 18 observers from 238 days before to 93 days after perihelion has been selected. Light curves for the 1978, 1984, 1990 and 1997 apparitions were previously

constructed and described by Sekanina (2003). In the two latter cases our light curves are very similar to Sekanina's, differing only slightly in the numbers of utilized measurements.

Sekanina (2003) showed that the comet was about equally bright in 1978, 1984, and 1997, but at least one magnitude fainter in 1990. He suggested a relation of this fall in brightness to a moderate change of the orbit due to an approach of the comet to Jupiter in 1987. The perihelion distance thus increased from 1.5 AU in 1984 to 1.6 AU in 1990. In the next apparition in 1997 the perihelion distance remained the same, but the brightness of the comet recovered to the level of the 1978 apparition.

As already mentioned, we confirm Sekanina's finding regarding the 1990 and 1997 light curves. Applying a shift to the 1990 light curve to make it fit with that of 1997, we also confirm Sekanina's conclusion that the composite light curve for 1978–1997 is not symmetric with respect to perihelion as far as the 1990–1997 period is concerned. As noted by Sekanina, the pre-perihelion branch is steeper than the post-perihelion one and the maximum brightness that we deduce occurs about 30 days before perihelion.

2.3. Estimates of gas production rate

We have translated each visual magnitude observation into a water production rate Q_{H_2O} using an empirical law: $\log Q_{H_2O} = C - 0.24\, m_H$, where $C = 30.74 \pm 0.02$ was originally estimated by Jorda et al. (1992). However, we apply a different value of C that we established by comparing the level of the visual light curve in 1997 and the observed water production rates from the same apparition. The observed production rates consist of three sets of measurements provided by Fink et al. (1999) (spectroscopy of the ^{1}D line of atomic oxygen), Mäkinen et al. (2001) (Lyman-α measurements made with SWAN on board SOHO), and Farnham & Schleicher (2005) (narrowband photometry of the near-UV OH emission).

Observed water production rates versus time from perihelion are shown in Fig. 1 by big symbols with error bars. Apart from those of 1997, three estimates from 1984 provided by Farnham & Schleicher (2005) are also marked. There are large differences between the measurements, the SOHO data standing out especially when compared to the others – they differ by a factor two from the rates based on narrowband photometry. The Fink et al. estimates are in between, and because of this we used their maximum as a check on the magnitude-based production curve from 1997. Thus the value we obtain for C amounts to 30.50. Note that we have found a similar value ($C = 30.455$) in the case of comet 6P/d'Arrest (Szutowicz & Rickman 2006). In Fig. 1, the water production rates derived from the brightness measurements of the 1997 and 1990 apparitions are marked with small symbols. All data are consistent with a strong perihelion asymmetry. The water production rate from direct measurements peaks about 40–60 days before perihelion, while the magnitude-based production curves peak about 30 days before perihelion.

The quality of the observed water production rate sets limits on the estimation of the active area fraction on the nuclear surface. As indicated above, there is a substantial uncertainty of the maximum production rate for the 1997 apparition of comet 81P/Wild 2. The observational data provided by Farnham & Schleicher (2005) and by Fink et al. (1999) cover time intervals long enough to include the maximum of the production rate. According to these authors the peak value is approximately 1.1×10^{28} mol s^{-1} and 1.5×10^{28} mol s^{-1}, respectively. In both cases it seems to occur about 40–60 days before perihelion. Mäkinen et al.'s (2001) data set starts 44 days before perihelion,

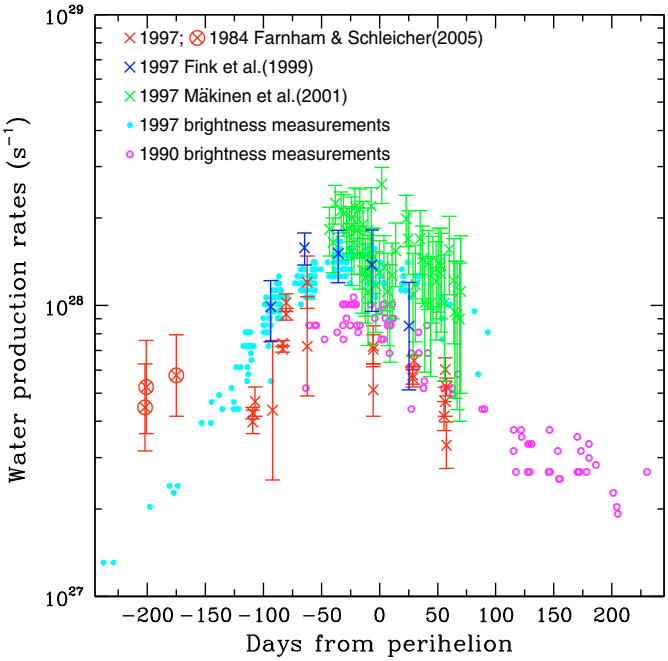

Fig. 1. Observed water production rates (marked with big symbols) and the brightness measurements for 1997 (magenta) and 1990 (cyan) converted into production rates.

i.e. after the maximum found by the other authors, and it extends to significantly higher values. The maximum of the latter data set is almost 2×10^{28} mol s^{-1}. The mean value of the three considered maxima is 1.5×10^{28} mol s^{-1}. We adopt this value as the basis for our evaluation of the active area. However, due to the large uncertainties of the measurements we have also established upper and lower limits for the maximum production rate. To this end, we consider the maximum of the Mäkinen et al. data plus their mean error as the upper limit (2.4×10^{28} mol s^{-1}), while the maximum of the Farnham and Schleicher data minus their mean error is the lower limit (9.6×10^{27} mol s^{-1}).

2.4. The nucleus – size, orientation, location of active regions

Images taken by the Stardust spacecraft during its flyby of comet 81P/Wild 2 show the nucleus with an active surface, and its shape is approximated by a triaxial ellipsoid with semi-axes: $a = 2.75$ km, $b = 2.00$ km and $c = 1.65$ km (Brownlee et al. 2004). For the spotty model considered in the present work the shape model is not crucial, and the size of the nucleus is mostly employed to estimate the bulk density of the nucleus.

The spatial orientation of the comet has been studied by several authors. We cite a few estimations of the spin axis orientation from the literature. They were converted, whenever necessary, into the Eulerian angles applied by Sekanina (1981). In his notation, the equatorial obliquity (I) is the angle between the orbital and equatorial planes of the comet, and the cometocentric solar longitude at perihelion (ϕ) is measured from the vernal equinox of the comet in the sense of increasing true anomaly ϑ to the sub-solar meridian at perihelion.

The spin axis orientation $(I, \phi) = (56° \pm 7°, 167° \pm 6°)$ was derived by Farnham & Schleicher (2005) based on analysis of the fan direction in 1997, while Sekanina (2003) – using similar data for the same apparition – found $(I, \phi) = (75°, 150°)$. On the other hand, Sekanina et al. (2004) estimated the orientation $(I, \phi) = (55°, 150°)$ after fitting of a triaxial ellipsoid to the

Table 3. Isotropic model – physical parameters of a rotating nucleus for comet 81P/Wild 2 obtained from various linkages.

Symmetric non-gravitational model; standard $g(r)$						
Interval	$A[10^{-8}$AU day$^{-2}]$	η	$I_0{}^a$	$\phi_0{}^a$	τ [days]	rms
1978–1984–1990	0.1046 ± 0.0121	60.°95±6.°03	81.°54±3.°78	224.°00±7.°29	0	1.″18
1984–1990–1997	0.1690 ± 0.0109	41.°29±3.°52	82.°63±1.°40	175.°20±9.°12	0	1.″03
1990–1997–2003	0.1392 ± 0.0068	34.°97±3.°12	81.°08±0.°98	157.°87±9.°75	0	0.″73
1978–1984–1990–1997	0.1444 ± 0.0071	29.°47±6.°04	78.°10±3.°04	249.°04±4.°32	0	1.″17
1984–1990–1997–2003	undeterminable for $\tau = 0$					
Asymmetric non-gravitational model; $g(r[t-\tau])$						
Interval	$A[10^{-8}$AU day$^{-2}]$	η	$I_0{}^a$	$\phi_0{}^a$	τ [days]	rms
1978–1984–1990	0.1086 ± 0.0123	69.°87 ±1 5.°63	81.°48 ± 3.°55	231.°33 ± 8.°63	−23.76 ± 19.45	1.″18
1984–1990–1997	0.1387 ± 0.0090	61.°00 ± 4.°24	68.°22 ± 2.°25	219.°46 ± 8.°43	−111.26 ± 9.26	0.″91
1990–1997–2003	0.1601 ± 0.0065	42.°37 ± 2.°63	72.°13 ± 1.°97	230.°41 ± 7.°27	−77.48 ± 5.19	0.″65
1978–1984–1990–1997	0.1542 ± 0.0076	37.°14 ± 3.°57	70.°64 ± 2.°75	248.°81 ± 4.°41	−52.36 ± 5.11	1.″12
1984–1990–1997–2003	0.1581 ± 0.0056	56.°90 ± 1.°76	73.°12 ± 1.°24	229.°57 ± 4.°69	−101.60 ± 5.02	0.″84

[a] The epoch of I_0 and ϕ_0 is 2005 Jan. 30 TT.

Stardust images of the nucleus, while Brownlee et al. (2004) and Duxbury et al. (2004) reported $(I, \phi) = (57°, 156°)$. According to summary of the orientation estimates presented by Davidsson & Gutiérrez (2006) as well as following Sekanina et al. (2004), the values of I and ϕ fall in the intervals (55°, 80°) and (150°, 167°), respectively.

Thus the orientation of the spin axis seems to be fairly well constrained. However, the sense of rotation as well as the rotational period of the comet is presently unknown. Sekanina et al. (2004) considered a possible retrograde sense of rotation, and if so the above quoted values would correspond to the south pole of the nucleus. They suggested a rotational period between 12^h and 24^h. The sense of rotation is found to be prograde in our calculations by finding both $I < 90°$ and generally positive values of the lag angle η of the effective outgassing behind the subsolar meridian. We have adopted 12^h and 24^h for the spin period in our analysis of the thermal lag. However, for our general purposes, the rotational period of the nucleus is not crucial.

Sekanina (2003) identified the presence of two active regions on the nucleus of comet Wild 2: source I – near the rotation pole (latitude +82°), and source II – on the opposite hemisphere closer to the equatorial plane (latitude −25°). He found effective sublimation areas of 4.5 km^2 for source I and 9.5 km^2 for source II. The outgassing area of the second region would thus be twice the size of source I. According to their analysis of the jets in the coma, Farnham & Schleicher (2005) found that the primary jet is roughly aligned with the spin axis. Thus the northern source would be located within about 15° of the pole, i.e., at a latitude higher than 75°, while the secondary jet originates on the southern hemisphere between −37° and −62°.

3. Non-gravitational acceleration – isotropic model

To estimate the non-gravitational force acting on a rotating spherical cometary nucleus with H_2O sublimation from the whole surface, the standard method may be used (Marsden et al. 1973). Elaborating on this model, the three standard parameters A_1, A_2 and A_3 may be expressed as functions of time by the relations: $A_i = A \cdot C_i(t)$, $i = 1, 2, 3$, where $C_i(t)$ are direction cosines for the non-gravitational force acting on a rotating cometary nucleus, which – in turn – depend on the angular parameters introduced in Sect. 2.4: η, I, and ϕ (Sitarski 1990).

The values of the parameters: A, η – the lag angle of the effective outgassing behind the subsolar meridian, I_0 – the obliquity of the orbital plane to the nucleus equator, and ϕ_o – the solar longitude at perihelion are presented in Table 3. For asymmetric models replacing the standard function $g(r)$ by $g(r[t-\tau])$ we list also the values of τ – the time shift of $g(r)$ with respect to perihelion. For each chosen time interval (three or four consecutive apparitions) these non-gravitational parameters were calculated along with six corrections to the orbital elements that are not given in Table 3. The mean residuals of the linkages are listed under the heading 'rms'. Considering the values I_0 and ϕ_0 listed in the table, which are otherwise denoted as I and ϕ, the subscript '0' indicates that we use the osculating orbital plane at the epoch. Since the orbital plane is perturbed, the values of I and ϕ at any other time will differ somewhat from those at the epoch, but our model assumes the spin axis to be fixed in an inertial frame.

Generally, the solutions obtained using the asymmetric non-gravitational acceleration model decrease the mean residuals in comparison to the symmetric model. However, even though the suggested asymmetry always goes in the right direction, it is often too large when compared with the observed brightness asymmetry of the comet. A similar behaviour was found in Paper I for the models with constant parameters A_1, A_2, A_3. In Sect. 2.3 we found that the production curve peaks about 40–60 days before perihelion. As seen in Table 3, only the linkages that include the first apparition in 1978 are in agreement with this asymmetry. However, the solutions for τ are seen to be generally unstable – like those for η. In this connection, one should note that the modeled shift of the outgassing maximum may differ from the observed shift, because both branches of the $g(r[t-\tau])$ function are symmetric, while the observed slopes of the comet Wild 2 light curve are strongly asymmetric (Sekanina 2003).

However, it is worth noticing three items visible in Table 3. First, the values of η are always large and differ substantially between different sets of observations. This might suggest that η varies strongly with time – something that is, however, hard to understand and suggestive of shortcomings in the

model assumptions. Second, all these angular models give relatively large equatorial obliquities in the range 68°–82°. Third, for symmetric models, it appears that ϕ decreases with time, which might indicate nucleus precession. However, the model of isotropic activity cannot be expected to give a realistic physical representation of the comet in view of the evidence of local active regions, and the problem of the η values may partly arise from this shortcoming.

4. Non-gravitational acceleration – spotty model

The model that we use builds on previous models described by Sekanina (1988, 2003) and Szutowicz (2000), and here we limit ourselves to a brief presentation. We consider two active spots located on the surface of the rotating nucleus, the other regions being inactive. The instantaneous spin state is pure rotation about a fixed axis.

The rate of ice sublimation from each active spot at any given time is a function of the distance of the comet from the Sun (r) and the Sun's zenith distance (z) at the spot in question. For a spherical nucleus z is identical to the angular distance from the spot to the subsolar point. The absorbed solar energy is spent on sublimation and thermal reradiation, but heat conduction into or from the interior of the nucleus is neglected. Thus the sublimation flux (Z) – in molecules per m^2 and s – from each spot varies diurnally as the nucleus rotates but symmetrically relative to the subsolar meridian. For this we use formulae developed by Sekanina (1988, 2003), which can be expressed as:

$$Z(z,r) = Z_o(r) \cdot \xi(z,r), \tag{1}$$

where $Z_o(r)$ is the water sublimation flux at the subsolar point, and ξ is the relative flux at the angular distance z from this point. We have $\xi(0,r) \equiv 1$, and for $z \neq 0$ we have generally: $0 \leq \xi < 1$. The dependence of ξ on r comes from the shift of the balance between sublimation and radiation in the energy budget – the larger the value of r, the quicker ξ falls toward zero with increasing z.

We consider the local, instantaneous contribution of each active spot to the non-gravitational acceleration to be proportional to the corresponding sublimation rate. However, our model does not account for the diurnal variation of these quantities. Instead, we consider the rotational average, assuming that the variation in r in the course of one spin period is always negligible. Thus we obtain for spot 'j' the diurnal average of the sublimation rate:

$$\langle Q_j \rangle(r) = \frac{1}{2\pi} S_j Z_o(r) \int_{-\theta_{cj}}^{+\theta_{cj}} \xi(z_j, r) \mathrm{d}\theta_j; \quad j = 1,2 \tag{2}$$

where θ is the hour angle of the Sun ($-\pi \leq \theta \leq \pi$), and θ_c is either the critical value where ξ drops to zero, or – in case it stays positive – we have $\theta_c = \pi$. This critical angle depends on the orbital position of the comet. When taking the integral, one has to consider that z_j depends on several angles: the equatorial obliquity (I), the solar longitude (λ), the latitude of the spot (β_j), and the solar hour angle (θ). Of these we treat I and β_j as constants, while λ varies with time t during the orbital motion of the comet, and θ varies with the rotational phase. We call S_j the emission area of the spot in question.

To get the components (a_1, a_2, a_3) of the non-gravitational acceleration in the radial, transverse and normal directions, respectively, we consider the contribution to this vector from spot 'j' to have an absolute value proportional to Q_j and direction cosines expressible as functions of I, $\lambda(t)$, β_j and a lag angle η. The meaning of the latter is that the acceleration vector together with the spin axis spans a plane that forms an angle η with the subsolar meridional plane. This is not consistent with the use of the symmetric function ξ in all other parts of our description of the acceleration vector, but at least if η is not very large, it is a reasonable approximation. Finally, note that $\lambda(t) = \phi + \vartheta(t)$, where ϑ is the true anomaly and ϕ is the solar longitude at perihelion.

Each component (a_i) of the acceleration vector is given by the sum of the two contributions from the two spots so that $a_i = (a_i)_1 + (a_i)_2$. Following Szutowicz (2000), we can formally write:

$$(a_i)_j = f_j A_o \cdot h(r) \cdot \langle K_i \rangle_j \left(\eta, I, \lambda, \beta_j, \theta_{cj}\right), \quad i = 1,2,3 \tag{3}$$

for $j = 1$ or 2, where $h(r)$ is a dimensionless representation of $Z_o(r)$ normalized to unity at $r = 1$ AU (Sekanina 1988; Szutowicz 2000), f_j is a dimensionless factor which expresses the non-gravitational acceleration in units of $A_o = 10^{-8}$ AU day^{-2} and is proportional to the emission area S_j (see Sect. 5), and

$$\langle K_i \rangle_j = \frac{1}{2\pi} \int_{-\theta_{cj}}^{+\theta_{cj}} \xi(z_j, r)\ C_i(\eta, I, \lambda, \beta_j, \theta_j)\, \mathrm{d}\theta_j \tag{4}$$

is the averaged product of the relative production rate and a directional cosine of the acceleration vector.

An analytical form of the non-gravitational acceleration such as given above allows a solution for the nucleus orientation, the location of the active regions or other parameters using partial derivatives in an orbit improvement procedure. In our orbital computations we solve for the model parameters by least-squares fitting of the model ephemeris to the astrometric positions of the comet. The values of the non-gravitational model parameters are always determined simultaneously with the orbital elements from the observational equations.

We use two variants of the spotty model, which differ in the treatment of the lag angle. In the first variant (called Model A) η is treated as a constant independent of the orbital position of the comet. The parameters in this case are: η, I, ϕ, β_1, β_2, f_1 and f_2. This involves five angular parameters – η, I, ϕ, β_1 and β_2 – while the two remaining ones (f_1 and f_2) are non-dimensional expressions for the magnitude of the non-gravitational acceleration. The other variant (called Model B) allows for a variation of the lag angle in dependence on the heliocentric distance. The physical reason for such a dependence has to do with heat transfer within the nucleus – again inconsistent with the assumptions made above – but, as long as η remains small over the observed part of the orbit, we are not introducing any large errors. Equation (3) is then replaced by:

$$(a_i)_j = f_j A_o \cdot h(r) \cdot \langle K_i \rangle_j \left(\eta(r,x), I, \lambda, \beta_j, \theta_{cj}\right), \ i = 1,2,3 \tag{5}$$

where x is a function of the thermal inertia and spin period (see Sect. 4.1). The parameters of variant B are x, I, ϕ, β_1, β_2, f_1 and f_2.

4.1. Thermal models

We have computed thermal models with a non-zero heat transfer in order to characterize the dependence of η on r. For this case we resort to very simple model nuclei, where the spin axis is perpendicular to the orbital plane, and there is only one active spot situated on the equator. These assumptions mean that the heat flow is only driven by the radial motion of the comet and not by any seasonal effects. Therefore the variation of η is symmetric with respect to perihelion.

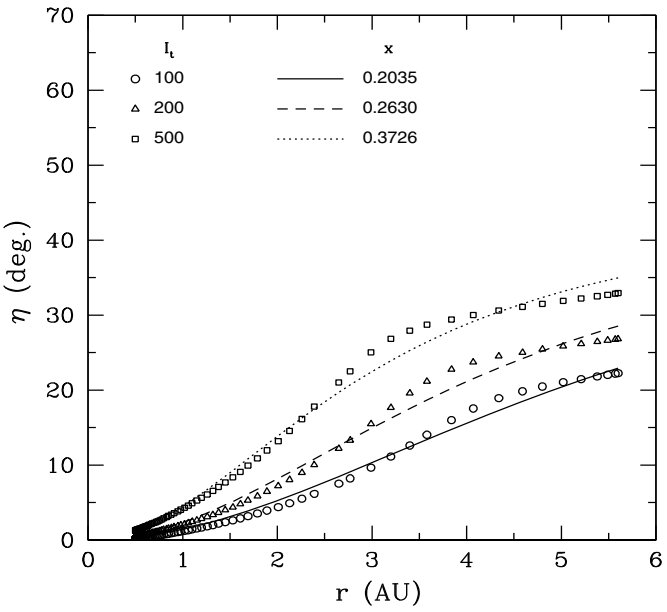

Fig. 2. Lag angle versus heliocentric distance derived from thermal models (marked by symbols) and from Eq. (6) (drawn by curves) for three different thermal inertias (in W $s^{1/2}$ m^{-2} K^{-1}). The spin period is 12^h.

The heat diffusion equation is first solved during the orbital motion, where a diurnal average of the insolation onto the active spot as a function of orbital position is used for the surface boundary condition, and next it is solved during the rotational period for selected orbital positions. The scheme of these thermal models is essentially the same as those developed by Froeschlé & Rickman (1986) and Rickman & Froeschlé (1986). The lag angle at each selected orbital position is found from the solution of the heat diffusion equation including a time-dependent surface boundary condition. We computed a number of models varying the thermal inertia I_t and spin period P_s in order to yield different variations of the lag angle.

The lag angle as a function of the heliocentric distance for three chosen thermal inertias (100, 200, 500 $Ws^{1/2}$ m^{-2} K^{-1}) and for $P_s = 12^h$ is shown in Fig. 2. The form of the heliocentric dependence of the lag angle was previously developed by Rickman et al. (1987):

$$\eta = 45^o \frac{x^2 r^2}{1.25 + x^2 r^2} \qquad (6)$$

where x is a dimensionless parameter that depends on thermal inertia and spin period. The lag angles calculated from each thermal model at different r were fitted by the least squares method to η as given by Eq. (6) in order to establish values of x. The resulting x values for a set of thermal models are listed in Table 4.

5. Results

We will only consider the results for the spotty models A and B, since we regard the results for the isotropic model – briefly described in Sect. 3 – as only a preamble with little potential for physical interpretations. In both cases A and B, it turned out impossible to solve for all the model parameters simultaneously. We thus had to fix at least one parameter, and this was usually chosen to be β_1, i.e., the latitude of the northern active spot. Moreover, linkage of all five apparitions – and four apparitions

Table 4. Values of the parameter x as a function of thermal inertia I_t and spin period P_s.

I_t [W $s^{1/2}$ m^{-2} K^{-1}]	Parameter x	
	for $P_s = 12^h$	for $P_s = 24^h$
100	0.2035 ± 0.0013	0.1767 ± 0.0010
200	0.2630 ± 0.0021	0.2321 ± 0.0017
300	0.3053 ± 0.0026	0.2692 ± 0.0022
500	0.3726 ± 0.0032	0.3264 ± 0.0029
900	0.4752 ± 0.0036	0.4134 ± 0.0035

too – is very problematic with the spotty model and will not be attempted here.

However, we have successfully linked the observations during three and two apparitions, starting from the last apparition with perihelion passage in 2003. We have also been able to derive more or less satisfactory non-gravitational linkages of three other groups of two or three apparitions as listed in Table 5. Acceptable fits for the three-apparition interval (2003–1997–1990) exist for several locations of the northern active source (Source 1) with latitudes from 78° to 86°. The orbital solutions with fixed values of β_1 within this range are practically identical, and here we present the one for $\beta_1 = 84°$. This value is chosen for all the linkages in Table 5. In particular, linking the interval (1997–1990–1984) successfully in a similar way requires the latitude of Source 1 to be $\beta_1 \approx 83°$–$85°$.

The values of all determined parameters have larger errors for the linkage including the 1984 apparition perhaps because this one involves rather few observations with a large a priori mean residual. The problem gets worse for the linkage of the interval (1990–1984–1978), where we could not find solutions without fixing three parameters. We thus assumed zero for the lag angle and we solved for I, ϕ, f_1 and f_2 with fixed β_2 or we solved for I, β_2, f_1 and f_2 with fixed ϕ. This time interval includes the first apparition of the comet after its capture from a much larger perihelion distance. Thus one may expect some instability in the pattern of the comet activity during this apparition.

Usually, to derive non-gravitational parameters from orbital linkages the minimal number of apparitions is three, since this allows to measure reliably the change of orbital period. However, the high quality of the astrometric observational material for comet 81P/Wild 2 allows measurement of the non-gravitational accelerations within a time frame of only two apparitions. The "a priori" mean residual for the apparitions in 2003, 1997 and 1990 is $0''.60$ (see Table 1). Purely gravitational fits to the observations at the two most recent apparitions (2003–1997) and at the two previous apparitions (1997–1990) yield residuals of $0''.72$ and $0''.75$, respectively, showing that such fits are clearly inferior to the non-gravitational ones presented in Table 5. We made two-apparitions linkages for the two mentioned intervals, assuming zero for the lag angle. In addition, for the interval (1997–1990) we could solve only for four parameters, and we had to fix either β_2 or ϕ in the same way as for the (1990–1984–1978) interval.

Note that the short-term linkages, as listed chronologically in Table 5, allow us to study the temporal variations of the non-gravitational effects. Consider for example the non-gravitational perturbation of the orbital period, ΔP. These perturbations per apparition within the investigated time intervals are listed in the last column of Table 5. The non-gravitational delay in the return of the comet to perihelion decreases from about 32 minutes to

Table 5. Two-source models – model parameters obtained from linkages of different sets of observations covering two or three apparitions.

Model A									
Interval	η	I_0^a	ϕ_0^a	β_1	β_2	f_1	f_2	rms	ΔP [min]
2003–1997	0.0	59.9 ± 2.4	155.5 ± 2.4	84°	-42.2 ± 1.2	0.502 ± 0.039	0.948 ± 0.072	0.″61	17 ± 6
2003–1997–1990	-0.3 ± 2.1	66.8 ± 1.6	154.3 ± 2.1	84°	-41.7 ± 1.7	0.426 ± 0.021	0.892 ± 0.043	0.″63	11 ± 3
1997–1990	0.0	78.1 ± 1.7	158.7	84°	-42.1 ± 0.9	0.425 ± 0.027	0.945 ± 0.068	0.″60	7 ± 5
	0.0	78.1 ± 1.6	158.7 ± 1.8	84°	-42.1	0.425 ± 0.030	0.944 ± 0.072	0.″60	7 ± 5
1997–1990–1984	1.1 ± 6.1	58.1 ± 4.0	148.9 ± 4.8	84°	-43.7 ± 6.5	0.328 ± 0.028	0.622 ± 0.050	0.″90	15 ± 5
1990–1984–1978	0.0	52.3 ± 7.5	134.6	84°	-30.3 ± 2.4	0.255 ± 0.039	0.677 ± 0.047	1.″17	32 ± 5
	0.0	52.5 ± 6.5	134.6 ± 6.6	84°	-30.3	0.256 ± 0.041	0.678 ± 0.056	1.″17	32 ± 4
Model B									
Interval	x	I_0^a	ϕ_0^a	β_1	β_2	f_1	f_2	rms	ΔP [min]
2003–1997–1990	0.197 ± 0.055	65.7 ± 2.0	157.5 ± 2.6	84°	-37.4 ± 2.3	0.408 ± 0.023	0.871 ± 0.049	0.″63	17 ± 4
1997–1990–1984	0.163 ± 0.146	56.4 ± 4.5	149.7 ± 4.8	84°	-41.2 ± 6.5	0.327 ± 0.025	0.603 ± 0.052	0.″89	18 ± 6

Orbital elements: Epoch 2005 Jan. 30 TT (Equinox: 2000.0)

Interval	Model	Perihelion time	q (AU)	e	ω	Ω	i
2003–1997–1990	**A**	2003 Sep. 25.9514	1.591021	0.538676	41.7803	136.1446	3.2397
2003–1997–1990	**B**	2003 Sep. 25.9512	1.591021	0.538676	41.7810	136.1438	3.2397

[a] Epochs of I_0 and ϕ_0 are: 2005 Jan. 30 TT, 1998 May 01 TT or 1988 Aug. 27 TT in dependence on the time interval.

7 min per revolution up to the mid-1990's and then increases to reach about 17 min during the last two apparitions. A sudden change of the non-gravitational perturbations, measured by the standard parameter A_2, between 1988 and 1998 was earlier noted by Sekanina (2003).

The two-source models appear to give a good physical picture of the nucleus during the time interval for which it was determined. However, we also see evidence in Table 5 that the parameters are evolving with time, and in particular ΔP is changing in a way that is not predicted by the model. Hence, the spotty model has no predictive capability outside its relevant time interval, and large residuals are generally found, when applying it to earlier or later apparitions.

The values of I_0 and ϕ_0 in Model A often differ by more than the extent of the error bars, when comparing different linkages, and the question then arises, whether this indicates a precession of the spin axis or shortcomings of our model. First, the stated uncertainties are 1σ errors, and thus most of the solutions can actually be regarded as consistent with each other. Moreover, they are also consistent with the spin axis orientation derived from Stardust data by Brownlee et al. (2004), Duxbury et al. (2004) and Sekanina et al. (2004), which makes us confident that they are realistic. Nonetheless, we have to realize that our model of the nucleus is a very primitive one – e.g., instead of just two active spots there may be a continuous distribution of activity over latitude, and effects of shape and topography that our spherical model neglects may also be of importance. It is possible that changes in the outgassing pattern of the real nucleus that our model does not capture may be partly responsible for the deviating data points, for example for the (1997–1990) linkage, where ΔP was at a minimum. As to the (1990–1984–1978) linkage, we note that this solution has also chosen a very different value of β_2, which should be correlated with the pole orientation. The root of the problem may be the low quality of the older astrometric data together with the shortcomings of our physical model.

The derived spin axis orientations after recalculation into the ecliptic coordinate system are shown in Fig. 3. For comparison, the orientations determined by Farnham & Schleicher (2005), Sekanina (2003), Chesley & Yeomans (2005), Duxbury et al. (2004) and Sekanina et al. (2004) are also marked. The latter two are determined from the Stardust images and they differ internally by 6.5. Our solutions generally fall within about 30° from the Stardust solutions with the larger deviations represented by the outliers mentioned above. The linkage of two recent apparitions tend to yield the best agreement with the Stardust data (within 3.2 and 6.8). At this point we should stress that there is an evolutionary pattern in the pole orientation that parallels the one of ΔP – the ecliptic co-latitude of the north pole and the axial obliquity reach maximal values simultaneously with the minimum of ΔP. We also include in Fig. 3 the pole coordinates derived by Chesley & Yeomans (2005) from an orbital fit using the Rotating Jet Model for the last three apparitions (1990–1997–2003). Their procedure was quite different from ours, since the latitudes of the two jet sources were fixed, and they solved only for the jet strengths using a grid of pole positions. The coordinates plotted and listed in their paper correspond to the best-fitting pole for such solutions. There is also a difference between the functional expression for the sublimation rate assumed in our paper and that adopted by Chesley and Yeomans.

The rotational evolution of comet Wild 2 and possible drift of its spin axis due to the outgassing-induced jet force was extensively studied by Gutiérrez & Davidsson (2007). They simulated the spin axis evolution assuming a random pattern of activity across a non-spherical nucleus that fulfils both the orbital and the rotational constraints. According to their results the most probable variation of the spin axis is 4°–8° per orbit, but some of the considered activity patterns lead to displacements of up to 20° per orbit. In all their simulations the spin axis evolves towards larger ecliptic longitudes. Thus they conclude that the

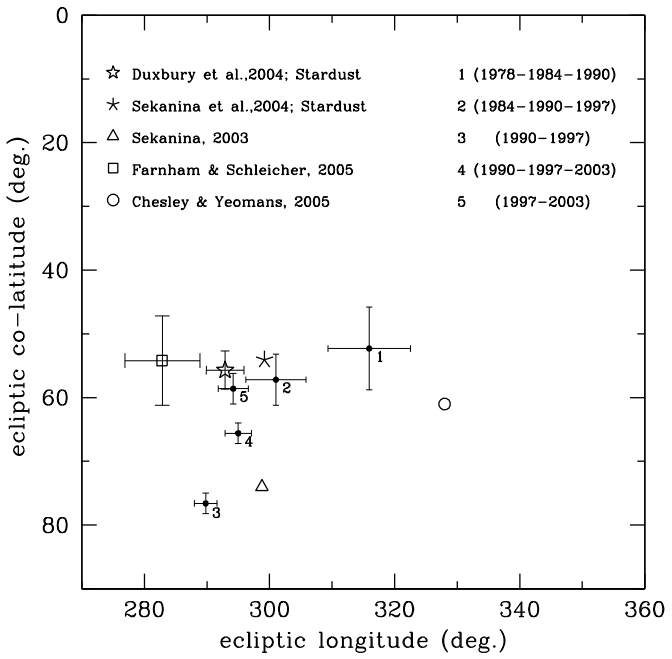

Fig. 3. Location of the spin axis in ecliptic coordinates. Symbols mark the spin axis orientations determined by previous authors, including those derived from Stardust data. Dots with error bars and digits denote the spin axis orientation derived from our orbital linkages of two or three apparitions.

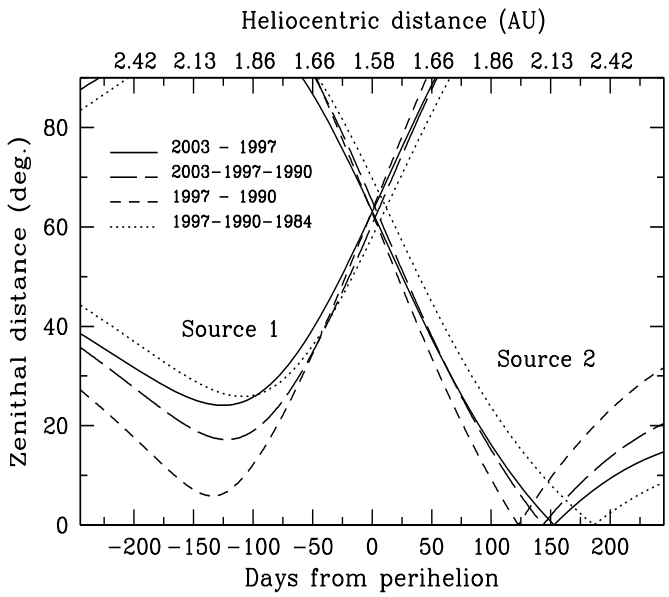

Fig. 4. Variations of the minimum solar zenith angle with the time from perihelion or heliocentric distance for the northern (1) and southern (2) active sources according to four different orbital linkages using Model A.

orientation for 1997 derived by Farnham & Schleicher (2005) is more likely than the one found by Sekanina (2003). We have also evolved the spin axis due to forced precession assuming the above-described two-source activity, and our result confirms that the spin axis drifts towards larger ecliptic longitudes as found by Gutiérrez & Davidsson (2007).

Our set of spin axis orientations, if taken at face value, would indicate a precessional pattern barely consistent with that predicted by forced precession. We conclude that the forced precession of the nucleus – whatever its rate may be – cannot be evidenced by our results. Both the limited amount and quality of astrometric data at older apparitions and the problems caused by unmodeled possible activity variations of the nucleus prevent us from doing so. Let us instead discuss the implications of our results in terms of possible changes in the outgassing areas of the sources.

In our model the intensity of the insolation depends both on the heliocentric distance and on the angle between the solar direction and the surface normal at the active spot. The variations of the minimum diurnal zenith angle of the Sun (at local noon) as a function of time from perihelion passage and heliocentric distance are plotted in Fig. 4. The plot illustrates the zenithal effect for the northern and southern source according to four orbital solutions derived from Model A. No curves are plotted for zenith distances larger than 90°, since then the spot receives no insolation.

The given orientations of the comet result in insolation of the northern source (at $\beta_1 = 84°$) before perihelion, while the southern source (at $\beta_2 \sim -42°$) is insolated after perihelion. However, the history of illumination differs between the axis orientations found for different linkages. Source 1 is most insolated for the (1997–1990) linkage, and in this case the Sun reaches Source 2 earlier than for the other linkages. Moreover, the insolation for the (2003–1997–1990) solution is generally stronger than for the (1997–1990–1984) solution.

We noted above that the dimensionless parameters f_j are proportional to the outgassing areas S_j, so we can write

$$f_j = \frac{S_j}{S}, \quad j = 1, 2 \tag{7}$$

in terms of a scaling factor S that has the dimension of an area. A physical interpretation of S is obtained from the expression of the non-gravitational force in terms of momentum flux and nuclear mass (Szutowicz 2000):

$$S = \frac{MA_o}{m\overline{u}Z_o(1\ \mathrm{AU})} \tag{8}$$

where M is the mass of the nucleus, m is the mass of a H_2O molecule, $\overline{u}$ is the outflow velocity of the molecules from the nucleus, and $Z_o(1\ \mathrm{AU}) = 1.52 \times 10^{28}$ molecules km^{-2} s^{-1} is the H_2O sublimation rate at the subsolar point at $r = 1$ AU. Another interpretation of S comes from observations of the H_2O production rate of the comet. In particular, if we concentrate on the maximum observed production rate $Q^{\mathrm{obs}}_{\mathrm{max}}$, we can identify this with the modeled production rate at the relevant orbital position as computed with Eq. (2):

$$Q^{\mathrm{mod}}_{\mathrm{max}} = S \cdot \frac{1}{2\pi} Z_o(r_{\mathrm{max}}) \sum_{j=1}^{2} f_j \int_{-\theta_{cj}}^{\theta_{cj}} \xi(z_j, r_{\mathrm{max}})\, \mathrm{d}\theta_j. \tag{9}$$

Using the values of f_j found from an orbital solution, one can then find S. From Eq. (7) one then finds S_j, and from Eq. (8) we can derive the mass of the nucleus.

The variations of insolation influence the modeled gas production curve, and at the same time we know from Eq. (8) that $S \propto M$ must be a uniquely determined constant (the mass of the nucleus does not vary significantly). Therefore it is important, when determining S from Eq. (9) using the value of $Q^{\mathrm{obs}}_{\mathrm{max}} = 1.5 \times 10^{28}$ s^{-1} derived in Sect. 2.3, to use the most relevant orbital linkage for evaluating the integrals. We deem this to be the (2003–1997–1990) linkage with its center at the well-observed 1997 apparition that dominates in our analysis of $Q^{\mathrm{obs}}_{\mathrm{max}}$.

Table 6. The areas of the two active regions based on non-gravitational solutions for different orbital linkages covering two or three apparitions.

Interval	S_1 [km^2]	S_2 [km^2]
Model A		
2003–1997	$4.9^{+3.0}_{-1.8}$	$9.3^{+5.6}_{-3.4}$
2003–1997–1990	$4.2^{+2.5}_{-1.5}$	$8.7^{+5.3}_{-3.2}$
1997–1990	$4.2^{+2.5}_{-1.5}$	$9.3^{+5.6}_{-3.3}$
1997–1990–1984	$3.2^{+1.9}_{-1.2}$	$6.1^{+3.7}_{-2.2}$
1990–1984–1978	$2.5^{+1.5}_{-0.9}$	$6.7^{+4.0}_{-2.4}$
Model B		
2003–1997–1990	$4.4^{+2.6}_{-1.6}$	$9.3^{+5.6}_{-3.4}$
1997–1990–1984	$3.5^{+2.1}_{-1.3}$	$6.5^{+3.9}_{-2.3}$

However, since we constructed two types of model (A and B) for this same interval, we get two different estimates of S. Our result for model A is $S = 9.8^{+5.9}_{-3.5}$ km^2, and for model B it is $S = 10.7^{+6.4}_{-3.8}$ km^2. The relatively large error bars reflect the uncertainty of the peak production rate in 1997.

Different linkages yield different values of f_1 and f_2, as seen from Table 5, and – using Eq. (7) – they hence yield different estimates of the outgassing areas S_1 and S_2. These results are listed in Table 6. Source 2 is about twice the size of Source 1 for almost all linkages – only the solution for (1990–1984–1978) gives 2.7 for the ratio S_2/S_1. For the most recent interval (1997–2003) our two-source model yields the areas 4.9 km^2 and 9.3 km^2, respectively. Thus the total active area is 14.2 km^2, i.e., it covers about 26% of the whole nucleus surface. For our standard interval the total active area is 12.9 km^2 (24% of the whole surface). Similar sizes of the outgassing areas (4.5 km^2 and 9.5 km^2) were found by Sekanina (2003).

Using the above values for S and adopting 0.6 km s^{-1} for the outflow speed of water molecules (Szutowicz & Rickman 2006), we estimate the mass of the nucleus to be $1.33^{+0.80}_{-0.48} \times 10^{13}$ kg according to model A, and $1.45^{+0.87}_{-0.52} \times 10^{13}$ kg for model B. To derive the bulk density we assumed the volume of the triaxial ellipsoid determined by Brownlee et al. (2004). Then the density is found as 350^{+210}_{-130} kg m^{-3} in model A and 380^{+230}_{-140} kg m^{-3} in model B. Since the two model results are practically equivalent within their error bars, we may state our resulting mass of the Wild 2 nucleus to be $1.4^{+0.8}_{-0.5} \times 10^{13}$ kg and the resulting density to be 0.4 ± 0.2 g cm^{-3}.

The values of the parameter x derived from Model B (see Table 5) allow us to establish constraints on the thermal inertia depending on the assumed spin period of the nucleus. We use the two spin periods of Table 4, and we use the tabular values of (I_t, x) in each case to find the value of I_t that corresponds to x. For the (2003 – 1997 – 1990) linkage the thermal inertia is thus found to be about 90 Ws$^{1/2}$m^{-2}K^{-1} or 130 Ws$^{1/2}$ m^{-2} K^{-1}, assuming the spin period to be 12^h or 24^h, respectively.

Knowing the source areas, we may draw the model production curve according to Eq. (2). The differences between four linkages with model A are shown in Fig. 5. Generally speaking, the whole production curve rises for the latest apparitions in agreement with the increase of the source areas (see Table 6). We note that the low activity level for the interval (1997–1990–1984) seems to agree with a similar tendency for the brightness estimations during the 1990 apparition (marked by black dots). For comparison we show by the dotted curve the production rate for the two-source model proposed by Sekanina (2003). Concerning the production curves of model B, they are quite similar to the ones for model A but show a slightly higher second maximum.

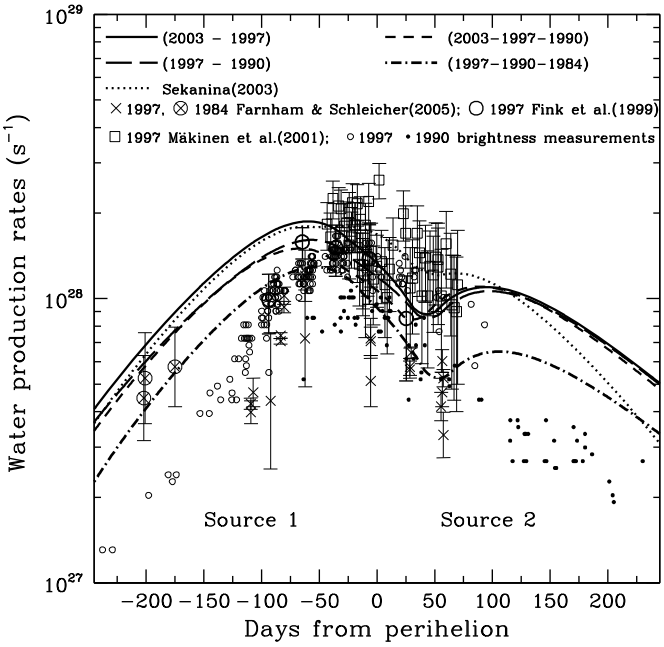

Fig. 5. Water production rate versus time for two-source model. Simulated production rates (marked with curves) within four different time intervals are derived from orbital solutions. The measured productions rates are denoted with different symbols (see Fig. 1).

6. Conclusions

Comet 81P/Wild 2 is an interesting object for physical studies, since it was recently captured into the observable Jupiter family and moreover, it was the target of NASA's Stardust mission. Thus several important properties of its nucleus are relatively well known, and others have been explored using physical models. In the present paper we took a further step in astrometric fitting by using a two-source model of the non-gravitational acceleration in orbital linkages.

As a preliminary step we computed a series of orbital solutions with an isotropically active nucleus, presented in Table 3. They made it clear that the orbital fitting prefers a non-gravitational force law that peaks before perihelion in agreement with most data on gas production rates for comet Wild 2. Such fits are of good quality, but the results for the time shift of the force law and the lag angle are rather unstable. The lag angles are very large and therefore suspect on the grounds of the common view that the thermal inertias of active cometary surfaces are very low.

Our two-spot models, presented in Table 5, gave totally different results in these respects. The lag angles – constant in model A and variable in model B – are always small, and the peak of the production curve is always about two months before perihelion in good agreement with the observed production rates. We were able to constrain the latitude of the northern spot to the vicinity of 84° N, and we used this value as fixed in all the solutions. The southern spot – the larger of the two – was found to be situated at about 40° S latitude.

We are aware that this two-spot model does not capture all the phenomena that are likely to be important on the real nucleus, but generally speaking, the spin axis orientation that we found is in good agreement with the results emerging from analysis of Stardust images. Our two-apparition linkage (1997–2003) results in the north pole orientation given by: longitude = 294.2° ± 2.4° and co-latitude =58.6° ± 2.4° in the ecliptic coordinates. Some apparent shifts of the spin axis between linkages that differ chronologically might be interpreted as forced precession but more likely result from the shortcomings of our model. However, we note that the evolution of the spin axis direction is correlated with time variations of the non-gravitational perturbation of the orbital period.

We determined the areas of the two source regions separately for each two- or three-apparition linkage and found that they have increased in agreement with a tendency for the 1990 visual magnitudes to suggest a lower production rate than observed during more recent apparitions. The total active area now seems to be about 14 km^2, or ~25% of the whole nucleus surface, with ~2/3 in the southern spot and ~1/3 in the northern one.

The mass of the nucleus was found, as a crude estimate, to be about 1.4×10^{13} kg corresponding to a bulk density of roughly 400 $kg\,m^{-3}$. An important contribution to the uncertainty of these estimates comes from the observed H_2O production rates. From our results for the lag angles we derived a thermal inertia of the order of 100 $Ws^{1/2}\,m^{-2}\,K^{-1}$. All these results are consistent with the picture of the cometary nucleus as a low-density, highly porous aggregate.

Finally, we emphasize that our determinations of all the physical parameters are based on the orbital calculations. Therefore, the agreement that we often find with earlier published data means that fitting astrometric observations by a non-gravitational force model provides a different and independent way to constrain the nuclear properties.

Acknowledgements. We are grateful to Grzegorz Sitarski for his helpful discussion on the numerical methods. We also thank the referee, Donald K. Yeomans for his valuable comments.

References

Brownlee, D. E., Horz, F., Newburn, R. L., et al. 2004, Science, 304, 1764
Chesley, S. R., & Yeomans, D. K. 2005, in Dynamics of Populations of Planetary Systems, ed. Z. Knežević & A. Milani, Proc. IAU Coll., 197, 377
Davidsson, B. J. R., & Gutiérrez, P. J. 2006, Icarus, 180, 224
Duxbury, T. C., Newburn, R. L., & Brownlee, D. E. 2004, JGR, 109, E12
Farnham, T. L., & Schleicher, D. G. 2005, Icarus, 173, 533
Fink, U., Hicks, M. P., & Fevig, R. A. 1999, Icarus, 141, 331
Froeschlé, C., & Rickman, H. 1986, A&A, 170, 161
Gutiérrez, P. J., & Davidsson, B. J. R. 2007, Icarus, 191, 651
Green, D. W. E. (ed.) 1991, ICQ, 77
Green, D. W. E. (ed.) 1997, ICQ, 97
Jorda, L., Crovisier, J., & Green, D. W. E. 1992, in Asteroids, Comets, Meteors 1991, ed. A. Harris & E. Bowell, 285
Królikowska, M., & Szutowicz, S. 2006, A&A, 448, 401
Mäkinen, J. T. T., Silén, J., Schmidt, W., et al. 2001, Icarus, 152, 268
Marsden, B. G., Sekanina, Z., & Yeomans, D. K. 1973, AJ, 78, 211
Rickman, H., & Froeschlé, C. 1986, A&A, 170, 145
Rickman, H., Kamél, L., Festou, M.C., & Froeschlé, C. 1987, ESA SP-278, 471
Sekanina, Z. 1981, Annu. Rev. Earth Planet. Sci., 9, 113
Sekanina, Z. 1988, AJ, 95, 911
Sekanina, Z. 2003, JGR, 108, SRD 2
Sekanina, Z., Brownlee, D. E., Economou, T. E., et al. 2004, Science, 304, 1769
Sitarski, G. 1984, Acta Astron., 34, 269
Sitarski, G. 1989, Acta Astron., 39, 345
Sitarski, G. 1990, Acta Astron., 40, 405
Sitarski, G. 2002, Acta Astron., 52, 471
Szutowicz, S. 2000, A&A, 363, 323
Szutowicz, S., & Rickman, H. 2006, Icarus, 185, 223